The Astrophysical Journal Letters, 828:L22 (7pp), 2016 September 10 doi:10.3847/2041-8205/828/2/L22


# ASASSN-16ae: A POWERFUL WHITE-LIGHT FLARE ON AN EARLY-L DWARF

Sarah J. Schmidt[1], Benjamin J. Shappee[2,10], Jonathan Gagné[3,11], K. Z. Stanek[4,5], José L. Prieto[6,7], Thomas W.-S. Holoien[4,5], C. S. Kochanek[4,5], Laura Chomiuk[8], Subo Dong[9], Mark Seibert[2], and Jay Strader[8]
[1] Leibniz-Institute for Astrophysics Potsdam (AIP), An der Sternwarte 16, D-14482, Potsdam, Germany; sjschmidt@aip.de
[2] Carnegie Observatories, 813 Santa Barbara Street, Pasadena, CA 91101, USA
[3] Department of Terrestrial Magnetism, Carnegie Institution of Washington, Washington, DC 20015, USA
[4] Department of Astronomy, Ohio State University, 140 West 18th Avenue, Columbus, OH 43210, USA
[5] Center for Cosmology and AstroParticle Physics, The Ohio State University, 191 W. Woodruff Avenue, Columbus, OH 43210, USA
[6] Núcleo de Astronomía de la Facultad de Ingenierá, Universidad Diego Portales, Av. Ejército 441, Santiago, Chile
[7] Millennium Institute of Astrophysics, Santiago, Chile
[8] Department of Physics and Astronomy, Michigan State University, East Lansing, MI 48824, USA
[9] Kavli Institute for Astronomy and Astrophysics, Peking University, Yi He Yuan Road 5, Hai Dian District, Beijing 100871, China
*Received 2016 May 13; revised 2016 July 28; accepted 2016 August 11; published 2016 September 9*

## ABSTRACT

We report the discovery and classification of SDSS J053341.43+001434.1 (SDSS0533), an early-L dwarf first discovered during a powerful $\Delta V < -11$ magnitude flare observed as part of the ASAS-SN survey. Optical and infrared spectroscopy indicate a spectral type of L0 with strong H$\alpha$ emission and a blue NIR spectral slope. Combining the photometric distance, proper motion, and radial velocity of SDSS0533 yields three-dimensional velocities of $(U, V, W) = (14 \pm 13, -35 \pm 14, -94 \pm 22)$ km s$^{-1}$, indicating that it is most likely part of the thick disk population and probably old. The three detections of SDSS0533 obtained during the flare are consistent with a total $V$-band flare energy of at least $4.9 \times 10^{33}$ erg (corresponding to a total thermal energy of at least $E_{\rm tot} > 3.7 \times 10^{34}$ erg), placing it among the strongest detected M dwarf flares. The presence of this powerful flare on an old L0 dwarf may indicate that stellar-type magnetic activity persists down to the end of the main sequence and on older ML transition dwarfs.

*Key words:* brown dwarfs – stars: chromospheres – stars: flare – stars: individual (SDSS J053341.43+001413.1) – stars: low-mass

## 1. INTRODUCTION

Magnetic activity, as traced by chromospheric H$\alpha$ emission, is ubiquitous at the transition between M and L spectral types (M7–L3; ML dwarfs). In more massive stars, this quiescent activity is often accompanied by flares, but observations of flares on ML dwarfs are relatively sparse. The flares that have been observed on late-M dwarfs are frequently dramatic, including those found in serendipitous spectroscopy (e.g., Liebert et al. 1999; Fuhrmeister & Schmitt 2004) and photometry (e.g., Rockenfeller et al. 2006; Schmidt et al. 2014a) in addition to some dedicated monitoring (e.g., Stelzer et al. 2006; Hilton 2011). While late-M dwarfs are significantly cooler than the earlier-M dwarfs and FGK stars where other flares were observed, observations have been consistent with a generally similar energy budget, with optical emission including both a thermal continuum and atomic (both line and continuum) emission (Schmidt et al. 2007).

Initial observations of L dwarf flares did not include the thermal white-light emission that is the hallmark of stellar flares, but were instead limited to sudden elevations in the H$\alpha$ emission without a thermal continuum (e.g., Hall 2002; Liebert et al. 2003). White-light flares have previously been detected on only one early-L dwarf: Gizis et al. (2013) found 21 flares in one quarter of *Kepler* short-cadence data from the L1 dwarf WISEP J190648.47+401106.8 (hereafter W1906). Additional detections of white-light flares are necessary to understand the changes in both the underlying magnetic dynamo and the interaction between the magnetic fields and the surface as we examine lower-mass, cooler objects.

On UT 2016 January 10, the ASAS-SN survey (Shappee et al. 2014) detected ASASSN-16ae (Shappee et al. 2016), a $\Delta V \sim -11$ magnitude event on SDSS J053341.43+001434.1 (hereafter SDSS0533), a source with ML dwarf colors. The detection of a flare this strong on a very low mass star is not only further evidence that strong magnetic activity extends to ultracool dwarfs (see, e.g., Rodríguez-Barrera et al. 2015; Pineda et al. 2016), but could have strong implications for the habitability of exoplanets found around ML dwarf hosts (Segura et al. 2010). In this Letter, we characterize the L dwarf source (Section 2) and the flare (Section 3) to place SDSS0533 in the context of magnetic activity on ML dwarfs.

## 2. CHARACTERIZING SDSS0533

We combine the ASAS-SN detections with survey data and additional observations to characterize the flare event and the quiescent properties of SDSS0533.

### 2.1. BVI Photometry

The ASAS-SN telescopes observe the entire sky roughly every other day. However, approximately half the sky (including SDSS0533) is observed at a slightly higher cadence because it is in the overlap region between multiple fields. As a result, there are $V$-band images taken ~2.9 hr before the flare, during the flare, and ~22 hr after the flare. The ASAS-SN fields were reduced using the standard ASAS-SN pipeline (B. J. Shappee 2016, in preparation). No source was detected in the

[10] Hubble Fellow.
[11] Sagan Fellow.

**Table 1**
Photometric Observations

| Date (UT) | Source | $N_{exp}$ | ET (s) | $B$ | $V$ | $I$ | $F_V$ |
|---|---|---|---|---|---|---|---|
| 2016 Jan 10 04:54:08 | ASAS-SN/Brutus | 2 | 90 | … | >16.74 | … | $<7.55 \times 10^{-16}$ |
| 2016 Jan 10 07:44:22 | ASAS-SN/Brutus | 1 | 90 | … | $13.51 \pm 0.02$ | … | $(1.48 \pm 0.03) \times 10^{-14}$ |
| 2016 Jan 10 07:46:10 | ASAS-SN/Brutus | 1 | 90 | … | $13.89 \pm 0.02$ | … | $(1.04 \pm 0.02) \times 10^{-14}$ |
| 2016 Jan 10 07:47:58 | ASAS-SN/Brutus | 1 | 90 | … | $14.16 \pm 0.03$ | … | $(8.12 \pm 0.22) \times 10^{-15}$ |
| 2016 Jan 11 01:16:04 | duPont | 1 | 60 | … | … | $19.15 \pm 0.03$ | … |
| 2016 Jan 11 01:19:55 | duPont | 1 | 180 | … | $22.77 \pm 0.17$ | … | $(2.92 \pm 0.46) \times 10^{-18}$ |
| 2016 Jan 11 01:25:04 | duPont | 1 | 180 | $23.31 \pm 0.20$ | … | … | … |
| 2016 Jan 11 06:01:31 | ASAS-SN/Cassius | 3 | 90 | … | >17.01 | … | $<5.88 \times 10^{-16}$ |
| 2016 Mar 29 00:34:32 | SOAR | 1 | 120 | … | … | $19.43 \pm 0.03$ | … |
| 2016 Mar 29 00:37:20 | SOAR | 2 | 180 | >24.54 | … | … | … |
| 2016 Mar 29 00:47:20 | SOAR | 1 | 360 | … | >24.19 | … | $<7.90 \times 10^{-19}$ |
| | adopted quiescent | | | … | $24.80 \pm 0.50$ | $19.43 \pm 0.03$ | $(4.51 \pm 2.07) \times 10^{-19}$ |

two individual pre-flare images[12] or the three individual post-flare images, so we combined each set of images.

We performed aperture photometry at the location of ASASSN-16ae using the IRAF `apphot` package and calibrated the results using the AAVSO Photometric All-Sky Survey (Henden & Munari 2014). We place 3σ upper limits on the pre- and post-flare epochs of $V > 16.7$ and $V > 17.0$, respectively, and find a sharp decline from $V = 13.5$ to $V = 14.16$ during the three individual flare images (see Figure 1 and Table 1). ASAS-SN detected no other flares from SDSS0533 in ∼1100 images acquired between 2012 January and 2016 March with *V*-band limiting magnitudes ranging from ∼15 to 18 depending on lunation and conditions.

We obtained two additional epochs of *BVI* photometry from the Wide Field Reimaging CCD Camera (WFCCD) on the duPont 100-inch telescope and the Goodman spectrograph (Clemens et al. 2004) on the Southern Astrophysical Research (SOAR) telescope. We performed aperture photometry on these images using the IRAF `apphot` package and calibrated the magnitudes using SDSS Data Release 10 (DR10; Ahn et al. 2014) photometry of nearby fields stars transformed into Bessel filters.[13] The source was detected on UT 2016 January 11 ($V = 22.77$), but the upper limit ($V < 24.19$) on UT 2016 March 29 indicates that the January 11 data were taken during a flare. It is unlikely that this detection was part of the ASASSN-16ae event because the largest stellar flares typically last $\lesssim$12 hr (Kowalski et al. 2010). It is possible they are related, however, because very large flares often trigger sympathetic flare events (Davenport et al. 2014). The magnitudes and 3σ upper limits are given in Table 1.

### 2.2. Survey Photometry

We obtained PSF photometry for SDSS0533 from the SDSS DR10 (Ahn et al. 2014) database as well as from the Two Micron All-Sky Survey (2MASS; Skrutskie et al. 2006) and the *Wide-field Infrared Survey Explorer* (*WISE*; Wright et al. 2010). The SDSS *iz*, 2MASS $JHK_S$, and *WISE* *W*1*W*2 are good quality, but the SDSS *ug* and *WISE* *W*3*W*4 magnitudes are too faint to be reliable and are not included. The SDSS *r* magnitude is flagged to indicate the SDSS position is not accurate. We did not correct the survey photometry (given in Table 2) for extinction because SDSS0533 is in the foreground of dust clouds (see Section 2.5) and not likely to be heavily extincted.

### 2.3. Spectroscopic Observations

We obtained a medium-resolution ($R \sim 4800$) optical spectrum of SDSS0533 using the Magellan Echellette (MagE; Marshall et al. 2008) spectrograph on the Baade-Magellan 6.5-m telescope on 2016 January 16. The target was observed for three 1800 s exposures at an airmass of ∼1.16 under clear conditions with the 0.″85 slit and 0.″6–0.″7 seeing. The wavelength coverage of MagE is 3100–10000 Å, but the continuum was not detected at wavelengths bluer than ∼6200 Å. We extracted all echellette orders of both SDSS0533 and the flux standard LTT 3168 using the MagE pipeline[14] and flux calibrated the spectra with standard routines from the IRAF `Echelle` package. The wavelength solution was shifted by 0.23 Å based on the position of the [O I] 5577 telluric emission line, and a heliocentric velocity correction was applied. The MagE spectrum (shown in Figure 2) is consistent with an L0 spectral type.

The Hα emission line is present in two spectral orders of MagE data. We measure the equivalent width (EW) of Hα from both orders, obtaining EW = −29.3 Å and EW = −29.8 Å. We adopt the mean value and assign an uncertainty of 0.5 Å based on the range of the two observations. The EW corresponds to an activity strength of $\log(L_{H\alpha}/L\mathrm{bol}) = -4.1$, one order of magnitude stronger than the average value for L0 dwarfs (Schmidt et al. 2015).

We obtained near-infrared (NIR) spectroscopy for SDSS0533 with the Folded-port InfraRed Echellette (FIRE; Simcoe et al. 2013) at the Magellan Telescopes on UT 2016 January 22 (PI: Gagné). We used the high-throughput long-slit mode to obtain $R \sim 450$ across the 0.8–2.45 μm range. SDSS0533 was observed in eight 60 s exposures in an ABBA pattern at an airmass of 1.18. A0 HD 290958 was observed for telluric correction immediately after at a similar airmass (1.17). Standard calibrations were taken as described by Gagné et al. (2015). The data were reduced using an updated version of the IDL FIREHOSE pipeline, which was based on the MASE (Bochanski et al. 2009) and SpeXTool (Vacca et al. 2003; Cushing et al. 2004) packages (FireHose 2.0[15]; see Gagné et al.

[12] A third dithered image was taken, but SDSS0533 was ∼25″ off the detector.
[13] Transformations from http://www.sdss.org/dr12/algorithms/sdssUBVRITransform/#Lupton2005.
[14] http://code.obs.carnegiescience.edu/mage-pipeline
[15] Available at https://github.com/jgagneastro/FireHose_v2/tree/v2.0.

**Table 2**
Properties of SDSS0533

| Parameter | Value |
|---|---|
| **Photometric** | |
| $V$[a] | 24.80 ± 0.50 |
| $I$ | 19.43 ± 0.03 |
| $r$[b] | 22.44 ± 0.15 |
| $i$ | 20.75 ± 0.05 |
| $z$ | 18.87 ± 0.04 |
| $J$ | 16.38 ± 0.13 |
| $H$ | 16.15 ± 0.16 |
| $K_S$ | 15.47 ± 0.21 |
| $W1$ | 15.16 ± 0.04 |
| $W2$ | 15.07 ± 0.08 |
| **Spectroscopic** | |
| ST | L0 |
| Hα EW (Å) | 29.5 ± 0.5 |
| $\log(L_{H\alpha}/L_{bol})$[c] | −4.1 |
| $V_{rad}$ [km s$^{-1}$] | 67.3 ± 7.0 |
| **Derived** | |
| $d(M_i/i-z)$ [pc] | 80.3 ± 20.7 |
| $d(M_i/i-J)$ [pc] | 68.9 ± 22.1 |
| $d(M_i/i-K_S)$ [pc] | 100.1 ± 35.2 |
| $d(M_J/\mathrm{ST})$ [pc] | 89.4 ± 17.3 |
| $d(M_H/\mathrm{ST})$ [pc] | 115.2 ± 22.8 |
| $d(M_{KS}/\mathrm{ST})$ [pc] | 103.2 ± 22.7 |
| $d(M_{W1}/\mathrm{ST})$ [pc] | 103.5 ± 18.7 |
| $d(M_{W2}/\mathrm{ST})$ [pc] | 111.6 ± 20.4 |
| $d$(mean) [pc] | 96.5 ± 23.1 |
| $Z$ [pc] | −13.3 ± 6.8 |
| $\mu_\alpha$ [mas yr$^{-1}$] | −124.8 ± 13.6 |
| $\mu_\delta$ [mas yr$^{-1}$] | −156.6 ± 35.6 |
| $V_{tan}$ [km s$^{-1}$] | −114.6 ± 31.5 |
| $U$ [km s$^{-1}$] | 13.5 ± 13.4 |
| $V$ [km s$^{-1}$] | −35.0 ± 14.3 |
| $W$ [km s$^{-1}$] | −94.0 ± 21.5 |

**Notes.**
[a] Adopted; see Section 3.
[b] Centroid flag set.
[c] Using $\chi = 1.9 \times 10^{-6}$ Å$^{-1}$ from Schmidt et al. (2014a).

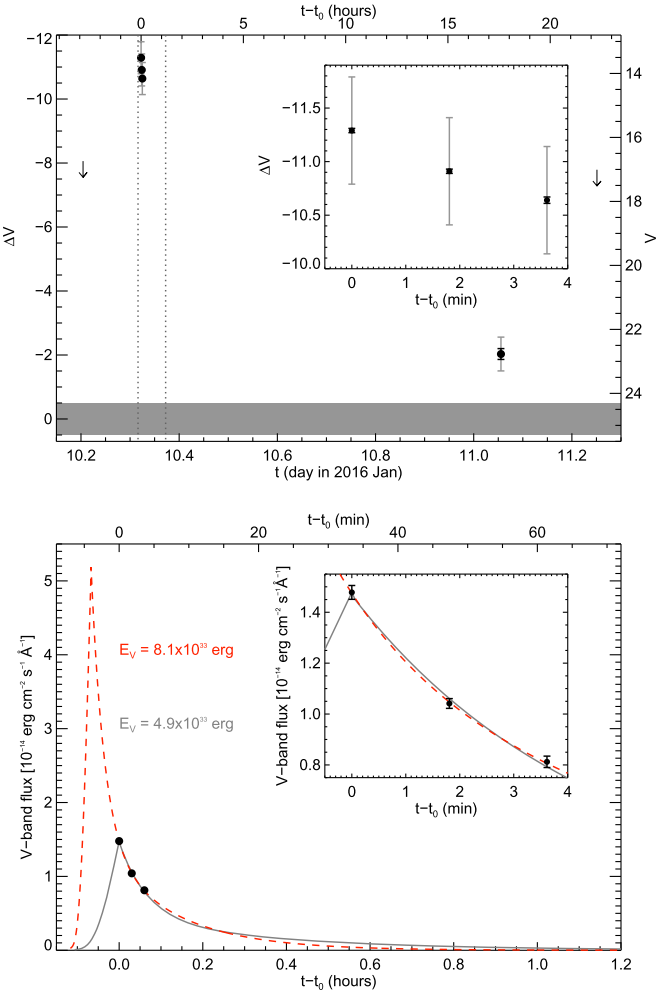


**Figure 1.** $V$-band detections of SDSS0533. Top: $\Delta V$ (left axis) and $V$ (right axis) as a function of time. The quiescent magnitude is shown with its uncertainty (gray shading) and individual detections are shown with photometric uncertainties (black error bars) and uncertainties in $\Delta V$ (gray error bars). The gray dotted line indicates the time included in the bottom panel. Bottom: $V$-band flux as a function of time with the minimum (gray solid) and best-fit (red dashed) empirical flare models (see Section 3.1). The inset panels show $\Delta V$ (top) and $V$-band flux (bottom) of the three flare detections.

2015). The spectral slopes of FIRE data are often unreliable due to de-centering of bright A0 standards to avoid saturation, so the slope of SDSS0533 was corrected to match its 2MASS photometry (see Gagné 2016). The final NIR spectrum is shown in Figure 2. Spectral indices (Allers & Liu 2013) and comparison to spectroscopic templates (Cruz 2016) indicate an L0 spectral type.

### 2.4. Kinematics

We estimated the distance to SDSS0533 using the photometric relations of S. J. Schmidt (2016, in preparation) and the spectroscopic relations of Dupuy & Liu (2012) assuming a spectral type of L0. The individual distance estimates vary from 68.9 to 111.6 pc (see Table 2), reflecting the intrinsic scatter of the relations as well as the slightly peculiar colors of SDSS0533. We adopt the mean distance of $d = 96.5 \pm 23.1$ pc. We calculated a proper motion of $\mu_\alpha = -124.8 \pm 13.6$ and $\mu_\delta = -156.6 \pm 35.6$ mas yr$^{-1}$ for SDSS0533 based on the 2MASS and AllWISE coordinates (the SDSS position was excluded due to poor centroiding). A search of the combined SDSS photometric database and USNO-B proper motions (Munn et al. 2004) reveals no nearby candidate companions. Combining the proper motion and the distance, we calculate a tangential velocity of $V_{tan} = -114.6 \pm 31.5$ km s$^{-1}$, well above the mean for early-L dwarfs ($V_{tan} = 28$ km s$^{-1}$; Schmidt et al. 2010).

We measured the radial velocity of SDSS0533 from the MagE optical spectrum via cross-correlation with the SDSS L0 template (Schmidt et al. 2014b) using five different ∼500 pixel regions in the sixth and seventh orders encompassing the region from 7150–8450 Å (avoiding telluric absorption at 7600 Å). The derived radial velocity, based on the mean and standard deviation of those values, is $V_{rad} = 67.3 \pm 7.0$ km s$^{-1}$. We calculated three-dimensional velocities of $(U, V, W) = (14 \pm 13, -35 \pm 14, -94 \pm 22)$ km s$^{-1}$, with uncertainties estimated using a Monte Carlo approach, assuming normal distributions for the errors in distance, $\mu$, and $v_{rad}$. The resulting kinematics (given in Table 2) include an unusually high $W$ velocity. Compared to the $W$ distributions of

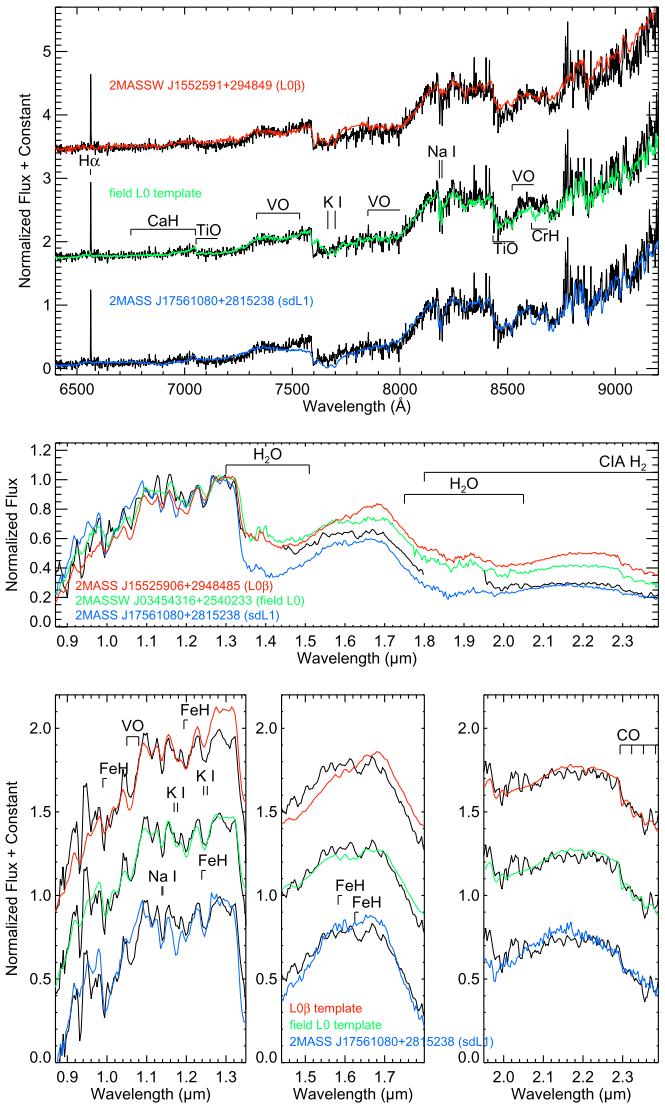


**Figure 2.** Spectra of SDSS0533 compared to templates, standards, and well-characterized L0/L1 dwarfs. The labeled spectral features were identified by Kirkpatrick et al. (1999) and Cushing et al. (2005), and the comparison spectra are discussed by Kirkpatrick et al. (2010), Schmidt et al. (2014b), and Cruz (2016). Top: the MagE optical spectrum (normalized at 8150 Å; black) compared to a low-gravity L0$\beta$ standard (red; Reid et al. 2008), the field L0 template (green; Schmidt et al. 2014b), and an sdL1 spectrum (blue; Kirkpatrick et al. 2010). Middle: the FIRE NIR spectrum (black) compared to a low-gravity L0$\beta$ standard (red; Allers & Liu 2013), a field L1 standard (green; Burgasser & McElwain 2006), and an sdL1 spectrum (blue). The spectra were normalized at 1.28 $\mu$m to facilitate comparison of the continuum slope. Bottom row: the FIRE NIR spectrum of SDSS0533 (black) compared to the Cruz (2016) low-gravity (L1$\beta$; red) and field (L1; green) templates and an sdL1 spectrum. The $zJ$, $H$, and $K$ bands are individually normalized to the full range displayed in each panel to facilitate comparison of individual features.

L dwarfs (Schmidt et al. 2010), SDSS0533 is ~5 standard deviations from the mean value for the thin disk, implying thick disk membership.

### 2.5. The Age of SDSS0533

SDSS0533 is located in the Orion constellation, within a few degrees of its vast star formation region (Genzel & Stutzki 1989). An association with Orion would imply a very young ($\lesssim$20 Myr) age, but at a distance of $d = 97$ pc (compared to $d \sim 400$ pc), SDSS0533 is more likely to be a foreground object and so neither within the dust cloud nor part of a young association. L dwarfs with ages $\lesssim$200 Myr can also be identified through spectral signatures of low gravity from their still contracting atmospheres; the optical and NIR spectra of SDSS0533 are not consistent with low-gravity (L0$\beta$) spectra, instead showing alkali lines, TiO bands, and a spectral slope similar to field-age L dwarf standards (Cruz et al. 2007; Cruz 2016). Spectral indices designed to identify low-gravity objects also indicate SDSS0533 is not young (gravity score of 0?00; Allers & Liu 2013).

While young L dwarfs often have red $J - K_S$ colors, SDSS0533 is blue ($J - K_S = 0.91$, compared to the L0 median of $J - K_S = 1.20$; Schmidt et al. 2015). Bluer $J - K_S$ colors are often associated with older ages, either due to a clearing of dust clouds, lower metallicity, or a combination of those two effects (Burgasser et al. 2008; Kirkpatrick et al. 2014). SDSS0533 has a similar NIR spectral slope to the low-metallicity sdL1 dwarf 2MASS J17561080+2815238 (Kirkpatrick et al. 2010), but lacks the unusually strong alkali lines and VO bands that are used to identify subdwarfs. Given its large $W$ velocity, SDSS0533 is most likely an older L dwarf (and consequently a star rather than a brown dwarf) with a near-solar metallicity and thin or patchy dust clouds.

## 3. PROPERTIES OF THE FLARE

The properties of the flare are sensitive to both the distance to SDSS0533 and its quiescent $V$-band magnitude. Our $V$-band photometry included only additional flares and upper limits, so we estimated a quiescent $V$-band magnitude based on photometry from Dieterich et al. (2014). M9.5–L0.5 dwarfs have a mean $M_V = 19.9 \pm 0.4$, $V - J = 8.2 \pm 0.2$, and $V - K_S = 9.5 \pm 0.2$. Based on the distance and $JK_S$ magnitudes of SDSS0533, we calculate $V = 24.8 \pm 0.5$, indicating an observed flare amplitude of $\Delta V = 11.3 \pm 0.5$ mag.

### 3.1. Fitting a Flare Shape

To estimate the shape of the flare, we employ the Davenport et al. (2014) empirical flare model based on *Kepler* short-cadence observations of the M4 dwarf GJ 1243. This empirical model was built using data from flares that occurred on a much warmer object (~900 K warmer) and so it is possible that ASASSN-16ae has fundamentally different energetics than the GJ 1243 flares. However, the only spectra of ML dwarf white-light flares (e.g., Schmidt et al. 2007; Gizis et al. 2013) are broadly consistent with those from M dwarfs (Kowalski et al. 2013), indicating a flare model from an M4 dwarf is suitable for estimating a flare energy.

The Davenport et al. (2014) model uses a double exponential to capture both the initial impulsive and the long gradual decay phases of a average flare that incorporates 885 classical (single-peaked) flares on GJ 1243. While the *Kepler* band samples a wider portion of the flare energy distribution than the $V$-band, both bands respond primarily to thermal flare emission (rather than atomic line or Balmer continuum emission; e.g., Kowalski et al. 2013), so their temporal evolution should be similar. The Davenport et al. (2014) model parameterizes flares based on the amplitude of the peak (here, peak $F_V$) and the time to half-light decay ($t_{1/2}$). Because our data only captures the decay phase, we also fit the time between the flare peak and the first detection ($t_{\rm det}$).

**Table 3**
Flare Model Properties

| Model | $t_{det}$ (s) | $t_{1/2}$ (s) | Peak $F_V$ (erg cm$^{-2}$ s$^{-1}$ Å$^{-1}$) | $\Delta V$ (mag) | ED (s) | $E_V$ (erg) |
|---|---|---|---|---|---|---|
| Minimum model | 0.0 | 384.0 | $1.48 \times 10^{-14}$ | −11.3 | $2.2 \times 10^{7}$ | $4.9 \times 10^{33}$ |
| Best fit | 241.0 | 178.5 | $5.19 \times 10^{-14}$ | −12.7 | $3.7 \times 10^{7}$ | $8.1 \times 10^{33}$ |

We generated one million flare light curves based on unique combinations spanning a range of peak $F_V$, $t_{1/2}$, and $t_{det}$, then quantified their fit to the data by minimizing the square to the difference between the model and the data divided by the uncertainties. We highlight two models: a minimum model that assumes the first flare detection is the peak value (adopting $t_{det} = 0$ and the first observed value for peak $F_V$) and the model with the best overall fit in all three parameters. The properties of both models are given in Table 3. The minimum model was selected to place a lower limit on the flare energy, but no strong upper limits can be placed on the flare energy because large flares often trigger sympathetic events in nearby magnetically active regions, resulting in long, multi-peaked emission events (e.g., Kowalski et al. 2010; Hawley et al. 2014).

### 3.2. Physical Properties of the Flare

We calculate the total energy emitted in the *V*-band during the flare by integrating across the model light curves; adopting the distance of $d = 97$ pc, we calculate a total energy of $E_V = 4.9 \times 10^{33}$ erg for the minimum model and $E_V = 8.1 \times 10^{33}$ erg for the best-fit model. The quiescent *V*-band luminosity of SDSS0533 is $L_V = 2.2 \times 10^{26}$ erg s$^{-1}$, indicating equivalent durations (EDs; time required to emit the flare energy during quiescence) of ED $= 2.2 \times 10^{7}$ s and $3.7 \times 10^{7}$ s, respectively. The *V*-band flare energy is also significantly larger than the bolometric luminosity ($\sim 1.0 \times 10^{30}$ erg s$^{-1}$ for spectral type L0; Filippazzo et al. 2015).

To compare this flare to those observed with *Kepler* on W1906, we adapt the Gizis et al. (2013) method of converting energy observed in a specific filter to total thermal energy by assuming the entirety of the flare energy is emitted in an 8000 K thermal spectrum. Due to the relatively cool temperature and the exclusion of atomic emission, this total thermal energy is a strong lower limit on the total flare energy. We calculate $E_{tot} = 7.7E_V$, indicating a total thermal energy of $E_{tot} = 3.7 \times 10^{34}$ erg for the minimum model and $E_{tot} = 6.3 \times 10^{34}$ erg for the best-fit model. These values both indicate this flare was ∼100 times larger than the most energetic flare observed on W1906.

Some of the largest flares on M dwarfs have been characterized in the *U*-band with $E_U \sim 2 \times 10^{34}$ erg (Hawley & Pettersen 1991; Kowalski et al. 2010). Adopting the Lacy et al. (1976) conversion of $E_U = 1.7E_V$, we calculate $E_U \sim 10^{34}$ erg, placing SDSS0533 on par with these energetic M dwarf flares. Like those flares, however, SDSS0533 is still less energetic than the largest stellar flares, which occur primarily on young F and G dwarfs (e.g., Davenport 2016).

We can also characterize the ASASSN-16ae event with a rough estimate of the size of the flare emission region. At optical wavelengths, white-light flares can be characterized by a combination of thermal (blackbody) and atomic (e.g., hydrogen Balmer) emission. The relative contribution of these two components and their characteristic temperatures change during the flare as the plasma cools. According to the detailed observations of Kowalski et al. (2013), thermal emission (characterized by temperatures of $T = 9000$–$14{,}000$ K) contributes 95% of the total flux during the impulsive phase, dropping to ∼50% of the total flux with characteristic temperatures of $T = 6000$–$10{,}000$ K during the gradual phase. To calculate a total flare area, we consider only the thermal emission; to convert total flare area to filling factor, we adopt a radius of $R = 0.105 \pm 0.007\,R_{\odot}$ (based on the radii of field M9–L1 dwarfs from Filippazzo et al. 2015). Due to the large flux of the flare, temperatures less than $T < 7000$ K are excluded as they would cover an area larger than the stellar disk.

If the observations occurred during the impulsive phase, the temperature range of $T = 9000$–$14{,}000$ K corresponds to total areas of 2.8–9.0 $\times 10^{19}$ cm$^{-2}$ (17%–54% of the surface). If the observations occurred during the gradual phase, the temperature range of $T = 7000$–$10{,}000$ K corresponds to total areas of 2.5–11 $\times 10^{19}$ cm$^{-2}$ (20%–68% of the surface). If the observations were instead taken during the transition from the impulsive phase to the gradual phase, as indicated by the model fit, intermediate temperatures and thermal contributions ($T = 9000$–$11{,}000$ K, ∼75%) correspond to total areas of 4.0–7.1 $\times 10^{19}$ cm$^{-2}$ (22%–40% of the surface). Overall, the total areas are similar to the largest mid-M dwarf flares, but the filling factors for ASASSN-16ae are much larger (>17% compared to <5%). In contrast, the filling factors of quiescent H$\alpha$ emission drop precipitously between mid-M and early-L dwarfs (Schmidt et al. 2015).

## 4. DISCUSSION

The detection of ASASSN-16ae is the first evidence that very powerful ($E \sim 10^{34}$ erg) white-light flares persist into the L spectral class and can occur on relatively old objects. If the flare frequency distribution of W1906 (Gizis et al. 2013) is typical of early-L dwarfs and can be extrapolated to higher energies, flares this large are likely to occur less frequently than on mid-M dwarfs: once every few years, compared to once or twice per month (Hawley et al. 2014). At comparable rates, ML dwarf flares could have a dramatic impact on the search for fast extragalactic transients (such as kilonova gravitational-wave counterparts; Cowperthwaite & Berger 2015; Kasen et al. 2015) in addition to a dramatic impact on their own magnetic evolution and any exoplanet companions.

To confirm the extrapolated L0 dwarf flare rate from W1906, we derive an order of magnitude estimate based on the ASAS-SN observations. ASAS-SN is likely to detect these powerful flares on L dwarfs as distant as 100 pc. Within that volume, we expect ∼5000 total L0 dwarfs (Cruz et al. 2003, 2007). ASAS-SN has taken an average of 500 images (90 s each) over the entire sky, indicating a total of $2 \times 10^{8}$ s (∼6 years) of L0 dwarf observations. With one flare detection, that yields a rate of one powerful flare on each L0 dwarf every six years, consistent with an extrapolation of the W1906 flare rate. At a

rate of ~1 flare per $10^8$ s, magnetic energy could be dissipated by flares this size ($E \sim 10^{34}$ erg) at an average rate of $10^{26}$ erg s$^{-1}$, or roughly $10^{-4}$ times the bolometric luminosity, placing energy release through flares on par with quiescent H$\alpha$ emission and one order of magnitude smaller than the X-ray emission.

The existence (and frequency) of dramatic flares on very small stars could also have strong a strong effect on the habitability of Earth-size planets around ML dwarfs, such as the recently discovered planetary system around M8 Trappist-1 (Gillon et al. 2016). Segura et al. (2010) found that the UV flux during large flares would be unlikely to affect habitable planets around flare star AD Leo, but habitable planets around ML dwarfs would be located ~4 times closer (0.024–0.049 au compared to 0.16 au), increasing the UV flux from flares by over an order of magnitude. Persistent UV flux could also interfere with the detection of biosignatures on a habitable world (Rugheimer et al. 2015). A better understanding of magnetic activity on ML dwarfs could be essential to the detection and characterization of nearby habitable exoplanets.

We thank the referee for useful comments that improved this Letter, and we thank Kelle L. Cruz for spectral templates, J. Davy Kirkpatrick for spectra, Jennifer van Saders for useful discussion, and LCOGT and its staff for continued support of ASAS-SN. ASAS-SN, as well as K.Z.S. and C.S.K., are supported by NSF grant AST-1515927. Development of ASAS-SN has been supported by NSF grant AST-0908816, the Center for Cosmology and AstroParticle Physics at the Ohio State University, the Mt. Cuba Astronomical Foundation, and George Skestos.

B.J.S. is supported by NASA through Hubble Fellowship grant HST-HF-51348.001 awarded by the Space Telescope Science Institute, which is operated by the Association of Universities for Research in Astronomy, Inc., for NASA, under contract NAS 5-26555. T.W.-S.H. is supported by the DOE Computational Science Graduate Fellowship, grant number DE-FG02-97ER25308. Support for J.L.P. is in part provided by FONDECYT through the grant 1151445 and by the Ministry of Economy, Development, and Tourism's Millennium Science Initiative through grant IC120009, awarded to The Millennium Institute of Astrophysics (MAS). S.D. is supported by "the Strategic Priority Research Program-The Emergence of Cosmological Structures" of the Chinese Academy of Sciences (grant No. XDB09000000) and Project 11573003 supported by NSFC. J.S. acknowledges support from the Packard Foundation.

Based in part on observations obtained at the Southern Astrophysical Research (SOAR) telescope, a joint project of the Ministério da Ciência, Tecnologia, e Inovação (MCTI) da República Federativa do Brasil, the U.S. National Optical Astronomy Observatory (NOAO), the University of North Carolina at Chapel Hill (UNC), and Michigan State University (MSU).

This research benefitted from the SpeX Prism Spectral Libraries (http://pono.ucsd.edu/~adam/browndwarfs/spexprism) maintained by Adam Burgasser and the Ultracool RIZzo Spectral Library (http://dx.doi.org/10.5281/zenodo.11313) maintained by Jonathan Gagné and Kelle Cruz.

This publication makes use of data products from the Two Micron All-Sky Survey, which is a joint project of the University of Massachusetts and the Infrared Processing and Analysis Center/California Institute of Technology, funded by the National Aeronautics and Space Administration and the National Science Foundation and from the *Wide-field Infrared Survey Explorer*, which is a joint project of the University of California, Los Angeles, and the Jet Propulsion Laboratory/California Institute of Technology, funded by the National Aeronautics and Space Administration.

This publication also makes use of data from the Sloan Digital Sky Survey. Funding for SDSS-III has been provided by the Alfred P. Sloan Foundation, the Participating Institutions, the National Science Foundation, and the U.S. Department of Energy Office of Science. The SDSS-III web site is http://www.sdss3.org/. SDSS-III is managed by the Astrophysical Research Consortium for the Participating Institutions (listed at http://www.sdss3.org/collaboration/boiler-plate.php).

## REFERENCES

Ahn, C. P., Alexandroff, R., Allende Prieto, C., et al. 2014, ApJS, 211, 17
Allers, K. N., & Liu, M. C. 2013, ApJ, 772, 79
Bochanski, J. J., Hennawi, J. F., Simcoe, R. A., et al. 2009, PASP, 121, 1409
Burgasser, A. J., Looper, D. L., Kirkpatrick, J. D., Cruz, K. L., & Swift, B. J. 2008, ApJ, 674, 451
Burgasser, A. J., & McElwain, M. W. 2006, AJ, 131, 1007
Clemens, J. C., Crain, J. A., & Anderson, R. 2004, Proc. SPIE, 5492, 331
Cowperthwaite, P. S., & Berger, E. 2015, ApJ, 814, 25
Cruz, K. L. 2016, AAS, submitted
Cruz, K. L., Reid, I. N., Kirkpatrick, J. D., et al. 2007, AJ, 133, 439
Cruz, K. L., Reid, I. N., Liebert, J., Kirkpatrick, J. D., & Lowrance, P. J. 2003, AJ, 126, 2421
Cushing, M. C., Rayner, J. T., & Vacca, W. D. 2005, ApJ, 623, 1115
Cushing, M. C., Vacca, W. D., & Rayner, J. T. 2004, PASP, 116, 362
Davenport, J. R. A. 2016, ApJ, in press (arXiv:1607.03494)
Davenport, J. R. A., Hawley, S. L., Hebb, L., et al. 2014, ApJ, 797, 122
Dieterich, S. B., Henry, T. J., Jao, W.-C., et al. 2014, AJ, 147, 94
Dupuy, T. J., & Liu, M. C. 2012, ApJS, 201, 19
Filippazzo, J. C., Rice, E. L., Faherty, J., et al. 2015, ApJ, 810, 158
Fuhrmeister, B., & Schmitt, J. H. M. M. 2004, A&A, 420, 1079
Gagné, J. 2016, ApJS, submitted
Gagné, J., Faherty, J. K., Cruz, K. L., et al. 2015, ApJS, 219, 33
Gagné, J., Lambrides, E., Faherty, J. K., & Simcoe, R. 2015, FireHose_v2: Firehose v2.0, Zenodo, doi:10.5281/zenodo.18775
Genzel, R., & Stutzki, J. 1989, ARA&A, 27, 41
Gillon, M., Jehin, E., Lederer, S. M., et al. 2016, Natur, 533, 221
Gizis, J. E., Burgasser, A. J., Berger, E., et al. 2013, ApJ, 779, 172
Hall, P. B. 2002, ApJL, 564, L89
Hawley, S. L., Davenport, J. R. A., Kowalski, A. F., et al. 2014, ApJ, 797, 121
Hawley, S. L., & Pettersen, B. R. 1991, ApJ, 378, 725
Henden, A., & Munari, U. 2014, CoSka, 43, 518
Hilton, E. J. 2011, PhD thesis, Univ. Washington
Kasen, D., Fernández, R., & Metzger, B. D. 2015, MNRAS, 450, 1777
Kirkpatrick, J. D., Looper, D. L., Burgasser, A. J., et al. 2010, ApJS, 190, 100
Kirkpatrick, J. D., Reid, I. N., Liebert, J., et al. 1999, ApJ, 519, 802
Kirkpatrick, J. D., Schneider, A., Fajardo-Acosta, S., et al. 2014, ApJ, 783, 122
Kowalski, A. F., Hawley, S. L., Holtzman, J. A., Wisniewski, J. P., & Hilton, E. J. 2010, ApJL, 714, L98
Kowalski, A. F., Hawley, S. L., Wisniewski, J. P., et al. 2013, ApJS, 207, 15
Lacy, C. H., Moffett, T. J., & Evans, D. S. 1976, ApJS, 30, 85
Liebert, J., Kirkpatrick, J. D., Cruz, K. L., et al. 2003, AJ, 125, 343
Liebert, J., Kirkpatrick, J. D., Reid, I. N., & Fisher, M. D. 1999, ApJ, 519, 345
Marshall, J. L., Burles, S., Thompson, I. B., et al. 2008, Proc. SPIE, 7014, 701454
Munn, J. A., Monet, D. G., Levine, S. E., et al. 2004, AJ, 127, 3034
Pineda, J. S., Hallinan, G., Kirkpatrick, J. D., et al. 2016, ApJ, 826, 73
Reid, I. N., Cruz, K. L., Kirkpatrick, J. D., et al. 2008, AJ, 136, 1290
Rockenfeller, B., Bailer-Jones, C. A. L., Mundt, R., & Ibrahimov, M. A. 2006, MNRAS, 367, 407
Rodríguez-Barrera, M. I., Helling, C., Stark, C. R., & Rice, A. M. 2015, MNRAS, 454, 3977
Rugheimer, S., Kaltenegger, L., Segura, A., Linsky, J., & Mohanty, S. 2015, ApJ, 809, 57

Schmidt, S. J., Cruz, K. L., Bongiorno, B. J., Liebert, J., & Reid, I. N. 2007, AJ, 133, 2258
Schmidt, S. J., Hawley, S. L., West, A. A., et al. 2015, AJ, 149, 158
Schmidt, S. J., Prieto, J. L., Stanek, K. Z., et al. 2014a, ApJL, 781, L24
Schmidt, S. J., West, A. A., Bochanski, J. J., Hawley, S. L., & Kielty, C. 2014b, PASP, 126, 642
Schmidt, S. J., West, A. A., Hawley, S. L., & Pineda, J. S. 2010, AJ, 139, 1808
Segura, A., Walkowicz, L. M., Meadows, V., Kasting, J., & Hawley, S. 2010, AsBio, 10, 751
Shappee, B. J., Prieto, J. L., Grupe, D., et al. 2014, ApJ, 788, 48
Shappee, B. J., Stanek, K. Z., Schmidt, S., et al. 2016, ATel, 8553
Simcoe, R. A., Burgasser, A. J., Schechter, P. L., et al. 2013, PASP, 125, 270
Skrutskie, M. F., Cutri, R. M., Stiening, R., et al. 2006, AJ, 131, 1163
Stelzer, B., Schmitt, J. H. M. M., Micela, G., & Liefke, C. 2006, A&A, 460, L35
Vacca, W. D., Cushing, M. C., & Rayner, J. T. 2003, PASP, 115, 389
Wright, E. L., Eisenhardt, P. R. M., Mainzer, A. K., et al. 2010, AJ, 140, 1868